Tellus SERIES B CHEMICAL AND PHYSICAL METEOROLOGY
PUBLISHED BY THE INTERNATIONAL METEOROLOGICAL INSTITUTE IN STOCKHOLM

Tellus (2011), 63B, 843–859
Printed in Singapore. All rights reserved

TELLUS

Separating remote fetch and local mixing influences on vertical radon measurements in the lower atmosphere

By S. CHAMBERS*, A. G. WILLIAMS, W. ZAHOROWSKI, A. GRIFFITHS and J. CRAWFORD, *Australian Nuclear Science and Technology Organisation, Institute for Environmental Research, Locked Bag 2001, Kirrawee DC, NSW 2232, Australia*

(Manuscript received 2 March 2011; in final form 3 June 2011)

ABSTRACT

Two-point radon gradients provide a direct, unambiguous measure of near-surface atmospheric mixing. A 31-month data set of hourly radon measurements at 2 and 50 m is used to characterize the seasonality and diurnal variability of radon concentrations and gradients at a site near Sydney. Vertical differencing allows separation of remote (fetch-related) effects on measured radon concentrations from those due to diurnal variations in the strength and extent of vertical mixing. Diurnal composites, grouped according to the maximum nocturnal radon gradient ($\Delta C_{\max}$), reveal strong connections between radon, wind, temperature and mixing depth on subdiurnal timescales. Comparison of the bulk Richardson Number (Ri_{B}) and the turbulence kinetic energy (TKE) with the radon-derived bulk diffusivity (K_{B}) helps to elucidate the relationship between thermal stability, turbulence intensity and the resultant mixing. On nights with large $\Delta C_{\max}$, K_{B} and TKE levels are low and Ri_{B} is well above the 'critical' value. Conversely, when $\Delta C_{\max}$ is small, K_{B} and TKE levels are high and Ri_{B} is near zero. For intermediate $\Delta C_{\max}$, however, Ri_{B} remains small whereas TKE and K_{B} both indicate significantly reduced mixing. The relationship between stability and turbulence is therefore non-linear, with even mildly stable conditions being sufficient to suppress mixing.

1. Introduction

Predictions of weather and climate conditions at the Earth's surface are crucially reliant upon the fidelity of model parameterizations that represent the integrated behaviour of key physical processes responsible for transport and mixing in the atmospheric boundary layer (ABL). Distributions of greenhouse gases, aerosols and other atmospheric pollutants with respect to their natural or anthropogenic sources, as well as their removal through surface deposition, are also controlled by these same processes (Li, 1974; Dueñas et al., 1996).

However, scientific understanding of many aspects of atmospheric mixing and transport processes still requires substantial refinement, or even fundamental revision. At the surface, for even rudimentary investigations of atmospheric chemistry there is a need to improve our understanding of the processes controlling the spatial/temporal variability in vertical exchange rates between the roughness elements (forest, crops or buildings) and the atmosphere above (Trumbore et al., 1990; Ussler et al., 1994; Martens et al., 2004). In the stably stratified boundary layer (SBL), vertical mixing processes remain poorly understood, particularly in very stable conditions when surface inversions can be extremely shallow (10−20 m or less; e.g. Leach and Chandler, 1992; Fernando and Weil, 2010) and the thermodynamic structure of the lowest 50−100 m very complex (e.g. Sorbjan, 2006). In the daytime convective boundary layer, where trace gases and aerosols are vertically mixed over a much deeper layer (1–2 km) and can be transported relatively quickly over large distances, there is still much to learn about the processes of entrainment and vertical transport of trace gases in coupled cloud layers (Williams et al., 2011).

The naturally occurring, radioactive gas radon (^{222}Rn) is an ideal tracer for transport and mixing studies in the ABL. Radon is the only gaseous decay product of the Uranium-238 decay series. Its source is almost exclusively terrestrial (Wilkening and Clements, 1975; Turekian et al., 1977), with a relatively modest spatial variability in strength over ice-free surfaces (typically 15–25 mBq m^{-2} s^{-1}; Turekian et al., 1977; Lambert et al., 1982). Furthermore, temporal variations are mainly associated with changes in soil moisture content and periods of rapidly changing surface pressure (Israelsson, 1978; Gogolak and Beck, 1980; Griffiths et al., 2010), and for the purposes of vertical mixing studies can generally be considered to be negligible on diurnal timescales. Being a noble gas that is poorly

*Corresponding author.
e-mail: Scott.Chambers@ansto.gov.au
DOI: 10.1111/j.1600-0889.2011.00565.x

soluble in water, atmospheric radon is not susceptible to dry or wet removal mechanisms. In fact, radon's only significant atmospheric sink is radioactive decay, and its decay timescale is ideally suited to ABL mixing studies. Since its half-life of 3.8 d is much larger than turbulent timescales (<1 h), it can be considered a conservative tracer for mixing in the ABL. On the other hand, this half-life is sufficiently short to ensure that typical concentrations in the free troposphere are orders of magnitude lower than near-surface concentrations.

Since the pioneering studies using radon as an atmospheric tracer (e.g. Wigand and Wenk, 1928; Israël, 1951, and references therein), an extensive body of literature has been published regarding the use of single-height observations of radon (or radon progeny) as a tool for the investigation of atmospheric stability and the dilution effects of prevailing meteorology (e.g. Li, 1974; Israelsson, 1978; Guedalia et al., 1980; Allegrini et al., 1994; Dueñas et al., 1996; Kataoka et al., 2003; Perrino et al., 2008). Less common, however, have been tower-based investigations of radon gradients (Table 1).

Vertical radon profiles in the ABL correlate well with the strength of atmospheric mixing (Pearson and Moses, 1966; Hosler, 1969; Williams et al., 2011), and the advantages of an

Table 1. Summary of published tower-based gradient/profile studies of Radon-222 and radon progeny

Study/citation	Location	Method	Heights	Time resolution	Measurement period
Moses et al. (1960)	Argonne National Laboratory, Illinois, USA (inland)	Radon	0.3, 1, 5.7, 24 and 40 m	1 hourly	3 d
Sisigina (1964)	Russia (unspecified)	Radon	0.1, 25, 50, 75, 150 and 300 m	Intermittent	Summer and autumn 1960–1962
Fontan et al. (1966)	Seine-et-Oise, France (inland)	Radon & Progeny	1.5 and 30 m	2 hourly	2 months
Israël et al. (1966)	Aachen, Germany (inland)	Radon & Progeny	0.5, 2 and 4 m	1–3 hourly	Several months
Malakhov et al. (1966)	Moscow, Russia (inland)	Radon & Progeny	0, 5 and 10 m	2-h averages of 20 min samples	3 months (summer)
Pearson & Moses (1966)	Argonne National Laboratory, Illinois, USA (inland)	Radon	0.01, 0.5, 1, 2, 4, 8, 16 and 40 m	20 min samples at 1–1.5 hourly intervals	8 separate days between May and August
Servant (1966)	Saclay, France (inland)	Progeny	1, 15, 30 and 100 m	2 hourly	Report 27 d from 4 months
Hosler (1969)	Washington, D.C., USA (inland, semi-rural)	Progeny	1 and 91m	1–4 hour averages of 20 min samples	22 months
Cohen et al. (1972)	Philadelphia, USA (inland, complex terrain, semi-rural)	Radon	6.1, 61, 174, and 271 m	1 hourly	Report 383 h from 5 months continuous observations
Li (1974)	Philadelphia, USA (inland, complex terrain, semi-rural)	Radon	6.1, 61, 174 and 271 m	1 hourly	Report 10 d from >1-yr observations.
Druilhet et al. (1980)	Roissy, France (inland)	Radon	1.5, 30 and 100 m	2 hourly	2 yr
Gogolak and Beck (1980)	New York, USA (inland, complex terrain; and flat, coastal)	Progeny	1, 10 and 25 m	1 hourly	Report 4 d (focus on steady-state night/day conditions)
Trumbore et al. (1990)	Manaus, Brazil (inland, closed forest)	Radon	0.02, 3, 6, 19, 27 and 41 m	30 min samples, 3 h between profiles	8 complete profiles over 3 nights
Porstendorfer et al. (1991)	Göttingen, Germany (inland, rural)	Radon & Progeny	0.1, 1, 2 and 5 m	1–3 hourly	10 d
Leach and Chandler (1992)	Roxby Downs, Australia (inland)	Radon & Progeny	1.25, 2.5, 5 and 20 m	1 hourly	3 yr
Butterweck et al. (1994)	Göttingen, Germany (inland, rural)	Radon & Progeny	0.1, 1, 2 and 5 m	3 hourly	Report 1 month
Ussler et al. (1994)	Quebec, Canada (inland, open forest)	Radon	0.05, 1, 9.5 and 18.2 m	30 min	2 weeks
Martens et al. (2004)	Tapajós National Forest, Brazil	Radon	0.1, 0.3, 1, 3, 10.7, 32, 37 and 61 m	15 min averages of 1 min samples	Two 1-month campaigns

ability to directly observe vertical radon gradients have been demonstrated by theoretical investigations of eddy diffusivity (K) in the surface layer and the ABL (Jacobi and André, 1963; Beck and Gogolak, 1979; Kumar et al., 1999). The practical difficulties of measuring high-resolution (multiheight) profiles of radon make long-term measurements unrealistic; however, a sustainable and productive compromise is the two-point gradient approach, in which the radon concentration difference, ΔC, is measured across an atmospheric layer adjacent to the surface (Druilhet et al., 1980; Ussler et al., 1994). Two-point radon gradients provide a much more direct measure of vertical mixing than can be obtained by analysis of a time history of single-point surface-based concentrations; furthermore, the majority of background signals associated with horizontal advection and fetch-related source variations are automatically removed by the differencing process. Compared with more conventional alternatives for deriving eddy diffusivities, the use of two-point radon gradients is relatively simple (even for long-term, continuous implementation) and less restricted to ideal surface or meteorological conditions (Butterweck et al., 1994). Due to its long (3.8 d) half-life, there is no need to account for radioactive decay in hourly gradient observations (Hosler, 1969), and the assumption of a constant surface radon flux density is robust as the diurnal variability in the radon source term is typically much smaller than the variability in K (Malakhov et al., 1966; Hosler, 1969; Li, 1974).

The investigations summarized in Table 1 have targeted a wide range of surface types (from flat to complex terrain, as well as urban, rural and forested settings), and their profiles have extended to heights of between 5–271 m, using between two and eight sampling heights. However, the applicability of results from these studies to the analysis of diurnal mixing processes has without exception been compromised in one or more of the following ways: limited temporal coverage (only days, weeks or months); discontinuous observations (only several samples per day, or measurements targeting equilibrium conditions only); limited temporal resolution (observations often only 2–4 hourly); limited instrument sensitivity (lower limits of detection of 200 – 1000 mBq m^{-3}); choice of sampling heights (which would ideally range from the surface to above the first inversion on very stable nights); lack of detailed accompanying meteorological information; or the use of radon progeny under conditions of potential disequilibrium (near the surface, over complex terrain or under mixed meteorological conditions). The unique data set on which the current investigation is based is subject to none of these restrictions.

The main aim of this study is to demonstrate the utility of continuous radon gradient observations as a direct, unambiguous measure of near-surface mixing. Using a long-term data set of continuous hourly direct measurements of atmospheric radon at two heights over a topographically complex, mixed urban/natural surface, we will characterize observed patterns of radon concentrations and gradients in terms of variations in air mass fetch, prevailing meteorology and vertical mixing, on both seasonal and diurnal timescales. Focussing specifically on the nocturnal window, we will then examine what two-point radon gradient measurements can reveal regarding the relationship between thermal stability, turbulence and vertical mixing.

2. Site and Methods

2.1. Site characteristics

In late 2005 a pair of detectors was installed at the Australian Nuclear Science and Technology Organisation (ANSTO) headquarters at Lucas Heights (LH) (34°03′S, 150°59′E) for the continuous hourly monitoring of atmospheric radon concentrations at two heights. LH is 30 km southwest of Sydney and 18 km from the coast. Being at the southern edge of the Sydney metropolitan area, surface land use in the area is a mixture of suburban (mainly to the east and north) and natural vegetation (mainly to the south). Locally the topography is complex, with changes in elevation of 150 m within 1 km of the site. The measurement location is on top of a broad ridge, with significant slopes to the north and south. In the direct vicinity of the measurements, fetch conditions are highly heterogeneous. Immediately (30−80 m) to both the east and west there are low (1−2 storey) buildings; 100 m to the south there is natural eucalypt forest; and to the north, the site is adjacent to grassed playing fields.

2.2. Radon instrumentation

Identical 1500 L dual flow loop two filter radon detectors were used for both sampling heights. For information regarding the principle of operation of two filter detectors, the reader is referred to Zahorowski et al. (2005), Newstein et al. (1971) or Thomas and Leclare (1970). Two filter detectors have a slow (∼45 min) response time, which prevents them from being multiplexed for profile observations. However, they have an advantage over techniques for estimating radon from its short-lived progeny in that reported concentrations are independent of the degree of equilibrium between radon and its progeny, which varies strongly in space and time, and with surface conditions and prevailing meteorology (e.g. Moses et al., 1960; Israël et al., 1966). The lower limit of detection (LLD), defined as the concentration at which the relative counting error is 30%, was about 40 mBq m^{-3} for both detectors.

Radon sampling at LH was conducted on a 50 m tower with 50 mm intake lines and inverted ('gooseneck' style) sampling inlets positioned at 2 and 50 m above ground level (agl). To ensure that the gradient detectors performed as similarly as possible, the following precautions were taken in addition to standard installations:

(1) The detectors were shielded from direct sunlight in order to minimize internal temperature fluctuations.

(2) A stack blower was located upstream of each detector, resulting in higher and more consistent flow rates ($\sim$100 L min^{-1}) than with the standard internal blower, and ensuring an overpressure of 100 Pa was maintained throughout each ^{220}Rn delay chamber and detector. Overpressure in the sampling line reduces the likelihood of near-surface air (high in ^{220}Rn and ^{222}Rn) directly entering the detector should any small leaks develop in the system.

2.3. System calibration

Instrumental background checks were performed every 3 months. Among other factors, a detector's background signal is affected by a slow build-up of ^{210}Pb ($t_{1/2} = 22.3$ yr) on the second filter, which is approximately linear over several years. Periodic checks of the background-to-signal ratio help to indicate whether refurbishment of the detector's measurement head is necessary. Accurate characterization and removal of a detector's background is imperative for gradient measurements, particularly at near-coastal sites where radon concentrations can vary over several orders of magnitude.

The LH detectors were calibrated monthly by injecting radon (at 40–80 cc min^{-1}) from a Pylon source (21.2 $\pm$ 4% kBq Radium-226) traceable to NIST standards. Injection periods were scheduled to finish between 1400 and 1500 h, when ambient radon concentrations were lowest and the 2–50 m radon gradient was small (typically $<$ 200 mBq m^{-3}). This was done for two reasons: (a) to minimize the uncertainty in calibration gas concentration brought about by changes in radon concentration of the carrier gas (ambient air); and (b) to enable the net calibration peak magnitude to be determined from the ambient radon concentration measured by the other detector.

2.4. Supporting meteorological measurements

Temperature, relative humidity (Vaisala, HMP45C), wind speed and wind direction (Gill, 2-D windsonic), were recorded at 2, 10 and 50 m on the tower. Unless otherwise stated, reported wind speeds are from the 10 m level (U_{10}) and reported gradients of temperature and wind speed are between 2 and 50 m. Incoming short-wave radiation (LI-COR silicon pyranometer) and net radiation (REBS, Q7.1) were recorded at 10 m. Other parameters included atmospheric pressure, soil moisture, soil temperature, ground heat flux, rainfall and surface temperature. All climatological measurements were stored on a Campbell CR-1000 data logger as 10-min averages of 20-s readings and later aggregated to hourly values to match the radon observations.

Gill Solent sonic anemometers were also situated at 10 and 50 m to monitor the 3-D wind vector at 20 Hz. Turbulent quantities were subsequently derived over 30-min periods and then averaged to hourly values.

2.5. Data availability and categorizations

Due to periods of maintenance or malfunction, the 2 and 50 m radon detectors were only in simultaneous operation for approximately 2 yr and 7 months of the 4-yr period 2006–2009. Unless otherwise stated, the results presented will be based on all 31 months of available data.

A spectral analysis of hourly radon concentrations from all four sites in ANSTO's Sydney network (not shown) indicated that the largest signal variability for these near-surface measurements occurred on diurnal timescales. This is directly attributable to diurnal changes in the depth of the ABL (Hosler, 1968; Guedalia et al., 1980; Allegrini et al., 1994). Consequently, the characteristics and interpretation of radon concentrations and gradients will strongly depend on the part of the diurnal cycle being considered.

Throughout the following sections, results will be categorized using the following definitions (see Fig. 1):

(1) **Daily:** derived from all 24 hourly samples on the selected day;

(2) **afternoon minimum:** average of samples in the 1400–1700 h afternoon window, when the ABL is deepest, well mixed and typically unstable;

(3) **nocturnal maximum:** maximum value attained in the 3 h pre-dawn window, when the ABL is shallowest and usually stably stratified;

(4) **nocturnal window:** sunset to sunrise.

All times reported are in Australian Eastern Standard Time (UTC + 10 h) and the southern hemisphere definition of seasons has been adhered to (Summer, December–February; Autumn, March–May; Winter, June–August; Spring, September–October).

3. Results and discussion

3.1 Annual mean concentrations

The annual mean 2 and 50 m radon concentrations at LH were 2120 and 1670 mBq m^{-3}, respectively, with the difference being primarily due to radon accumulation near the ground when the atmosphere is stably stratified (the nocturnal bias). Depending on the topographic setting of a given site, there can be a substantial nocturnal bias on diurnal mean near-surface radon observations. For example, although 2 m radon concentrations at our sites in Muswellbrook (32°16′S, 150°53′E) and Goulburn (34°45′S, 149°42′E) tend to exhibit similar daytime values in autumn when terrestrial fetches are comparable (typically 2–3 Bq m^{-3}), concentrations under stable nocturnal conditions often differ by more than a factor of two. This is likely to be attributable to the fact that the Goulburn site is situated in a regional depression.

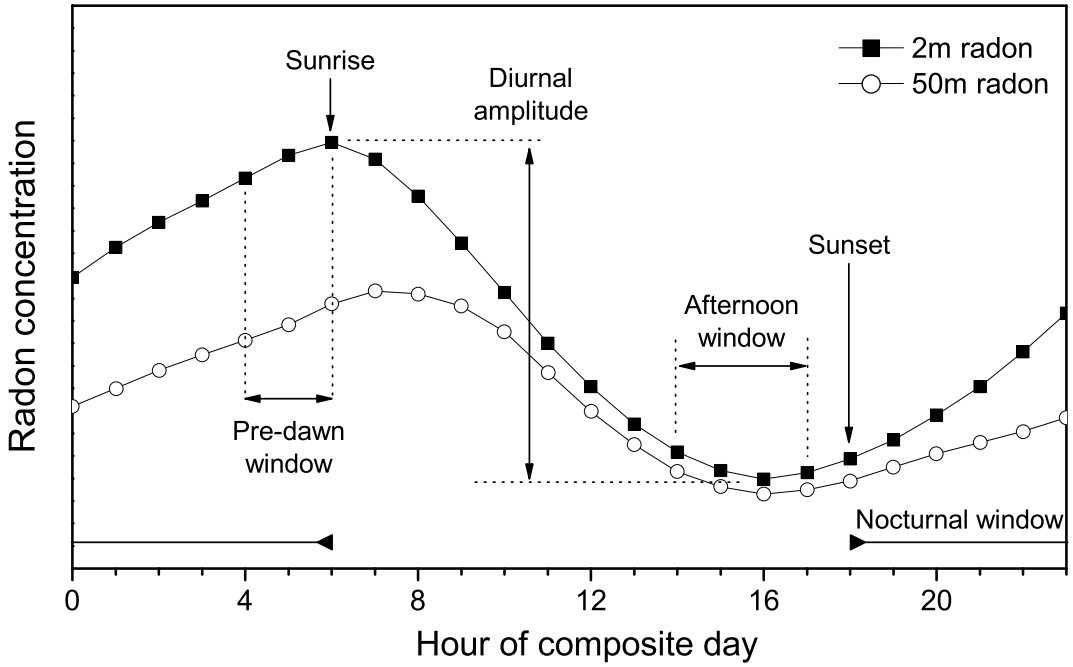

Fig. 1. Schematic of diurnal 2 and 50 m radon concentration time series with sampling windows annotated.

The nocturnal bias can be avoided by calculating the mean annual concentrations using only the afternoon minimum values (when mixing was typically strongest). This process yields annual means at 2 and 50 m of 1420 and 1260 mBq m^{-3}, respectively, in the present data set. The small residual difference (160 mBq m^{-3}) may indicate that non-negligible radon gradients can sometimes persist near the surface even in the middle of the day, a fact that has been noted by others (Pearson and Moses, 1966; Williams et al., 2011).

3.2 Seasonal variability in afternoon minimum radon concentration

A pronounced seasonal radon cycle is evident in the median monthly afternoon minimum radon concentrations at 50 m (Fig. 2). This statistic represents an approximation of the radon concentration within the deep afternoon mixed layer extending up to the main synoptic inversion, which changes slowly from day to day and is little affected by the transient behaviour of the near-surface nocturnal inversion. Broadly speaking, the

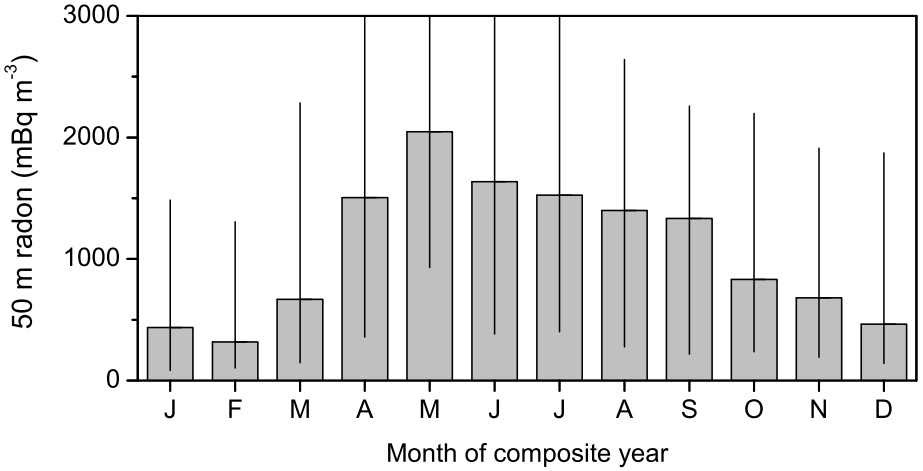

Fig. 2. Monthly distributions (10th, 50th and 90th percentiles) of afternoon minimum 50 m radon concentrations.

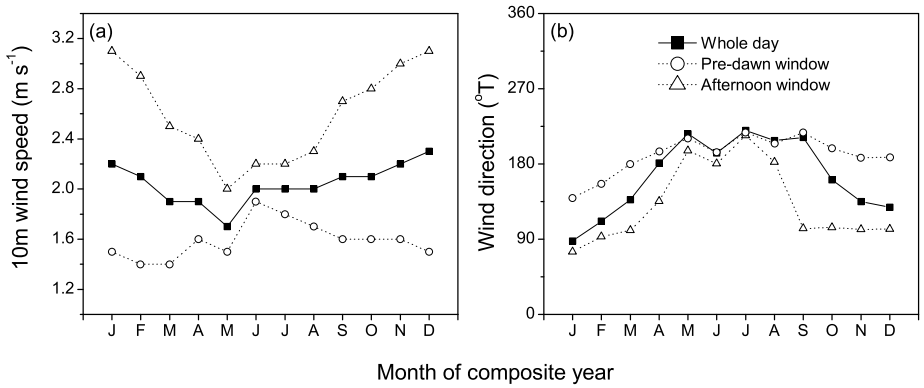

Fig. 3. (a) Mean monthly wind speed, and (b) mean monthly wind direction at Lucas Heights based on daily (closed squares), pre-dawn window (open circles) and afternoon window (open triangles) values.

observed cycle is dominated by high concentrations between April and September (peaking in May), and low concentrations in December–February. Four main competing factors contribute to the detailed features of the seasonal radon variability: air mass fetch, dilution within the ABL, contact time with land and variability in the radon source function (Hosler, 1968; Dueñas et al., 1996; Zahorowski et al., 2005; Williams et al., 2009). These are discussed separately later.

3.2.1. Air mass fetch. The magnitudes of observed radon concentrations at LH are strongly influenced by the (decay-adjusted) contributions of surface sources over which the air mass has travelled in the last week or two. In particular, the strength of the effective (integrated) source will depend on whether the air mass has passed over water or land (Wilkening and Clements, 1975) and, to a lesser degree, changes in regional geology (Griffiths et al., 2010).

A summary of the LH 10 m wind observations (Fig. 3) indicates a pronounced seasonality in air mass fetch. Between October and March, mean wind directions have a strong easterly component, indicating an oceanic fetch. Note also that the wind direction tends to swing from southeast at night to directly east in the day, indicating the influence of sea breezes. For the remaining months (April–September), the air mass fetch is dominated by land, with the highest proportion of land fetch occurring between July and September (mean wind directions south westerly).

Since the direction from which an air mass approaches a site is not always indicative of its recent fetch history, we also performed a seasonal analysis of 10-d air mass backtrajectories generated using HYSPLIT v4.0 (Draxler and Hess, 1998). Figure 4 depicts the results of a seasonal cluster analysis performed on daily 1400 h backtrajectories which had previously been truncated to 4 d. The ABL is typically well mixed at 1400 h, so a close correspondence is expected between the 50 m radon observations and the trajectory starting elevation of 500 m. Three seed trajectories per season were used for the clustering. The trajectory analysis confirms that air mass fetch at LH is predominantly oceanic in summer and terrestrial in winter, with autumn and spring being characterized by mixed fetch conditions. The observed variability in air mass fetch is pre-dominantly driven by the seasonal migration of the Southern Hemisphere subtropical ridge, which directs southeasterly flow towards LH in

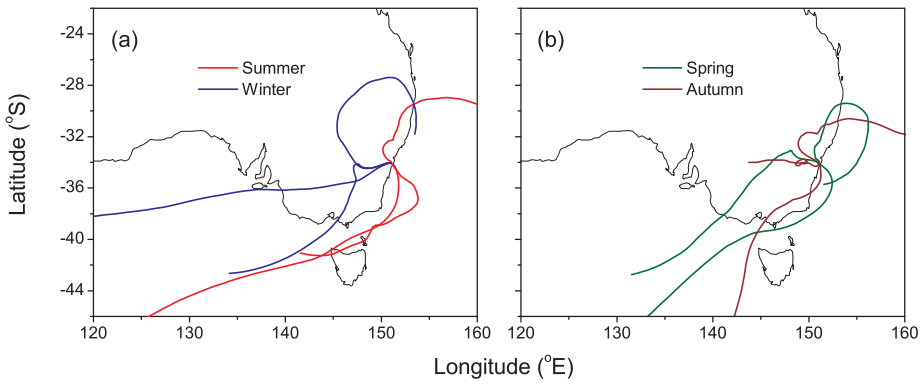

Fig. 4. Composite 1400 h back trajectories, truncated to 4 d, from Lucas Heights in (a) summer (red) and winter (blue), and (b) spring (green) and autumn (brown). Results are based on a cluster analysis of 10-d HYSPLIT backtrajectories, using three seed trajectories per season.

summer, south westerly flow in winter and variable light winds in May (http://www.bom.gov.au/jsp/ncc/climate_averages/mean-sealevel-pressure/index.jsp).

This dominant pattern of air masses switching from oceanic in summer to terrestrial in winter is broadly consistent with the seasonal cycle of afternoon radon concentrations as shown in Fig. 2. However, it is instructive to explore the contributions of other effects to the details of this distribution.

3.2.2. Dilution within the daytime ABL. For daytime observations, the synoptic (capping) inversion defines the mixing volume within which terrestrially emitted radon is diluted (Hosler, 1968; Guedalia et al., 1980; Hsu et al., 1980; Allegrini et al., 1994; Perrino et al., 2008). Consequently, seasonal variability in daytime ABL depth, brought about by changes in surface insolation, air mass fetch and other synoptic meteorological processes, will be reflected in corresponding near-surface radon concentrations.

The effect of ABL dilution can be largely eliminated by estimating the total column activity of radon at the measurement site,

$$R = \int_0^\infty C \mathrm{d}z \cong \langle C \rangle h, \tag{1}$$

where $\langle C \rangle$ is the mean radon concentration in the ABL and h is the ABL depth. Since tropospheric radon concentrations are typically an order of magnitude smaller than in the ABL (Williams et al., 2011), any radon above h has been neglected in this estimation.

We made daily estimates of R within the afternoon window by assuming radon to be well mixed throughout the ABL and equal to the concentration observed at 50 m, $\langle C \rangle = C_{50}$. The ABL depth, h, was estimated each afternoon using a bulk Richardson Number (Ri_B) approach (Holtslag and Boville, 1993) with virtual potential temperature and wind speed profiles from the Australian Bureau of Meteorology's regional LAPS model (Puri et al., 1998). Monthly distributions of R and h within the afternoon window are presented in Fig. 5a and 5b.

The seasonal cycle of R (Fig. 5a) is broadly similar in form to that of the afternoon radon concentrations (Fig. 2), with a couple of important differences. Relative to the overall shape of the distribution, median R-values are lower in April–July and higher in August–September. This creates a bimodal distribution in R, with peaks in April–May and August–September, and a local minimum in June–July. Although our wind and trajectory analyses (Figs 3 and 4) indicated shorter land fetches in autumn than in winter, relatively high column activities of radon were observed in April and May. This is likely to be attributable to a greater contact time with land due to lower wind speeds in autumn (Fig. 3a).

3.2.3. Contact with the land surface. To pick up radon, an air mass needs to be in contact with the land surface on approach to the measurement point. The length of contact time is a function of air mass fetch, velocity and altitude. In the absence of active, convective clouds, an air mass travelling significantly above the ABL inversion is not considered to be 'in contact' with land (Williams et al., 2011), even though it is travelling over land.

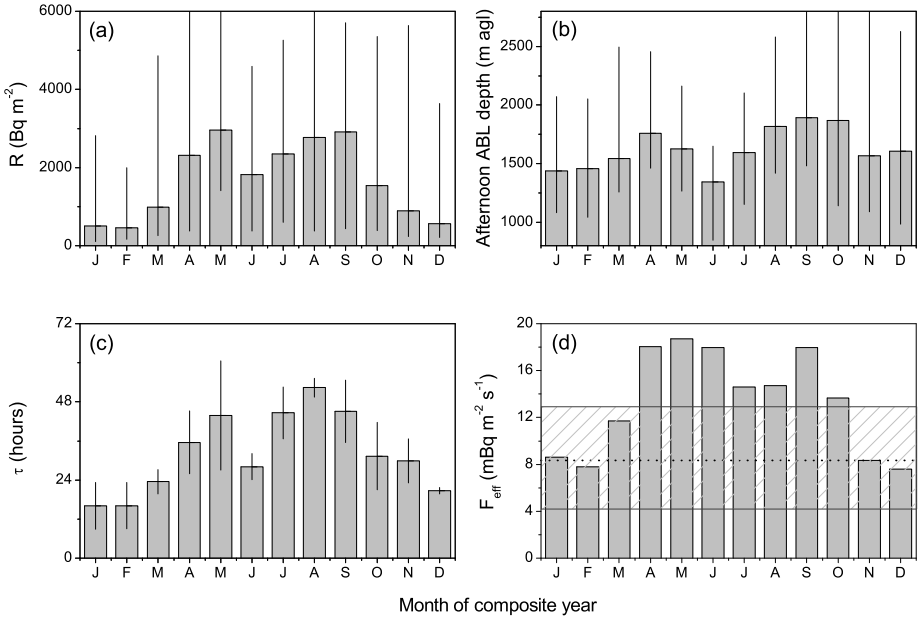

Fig. 5. Monthly distributions of (a) radon total column activity, R (10th/50th/90th percentiles), (b) LAPS afternoon boundary layer depth, h (10th/50th/90th percentiles), (c) distance-weighted time over land, τ (mean and standard deviations) derived from 10-d backtrajectories at 6-hourly intervals and (d) mean effective distance-weighted radon flux density, F_{eff} (hashed area represents mean $\pm$ *SD* LH flux density measurements).

We analysed the 10-d LH back trajectories for the time spent 'in contact' with land. An air mass was deemed to be in contact with land if its HYSPLIT trajectory was both over land (as determined using a 0.5 × 1° resolution map of Australia) and travelling at an elevation of less than 2000 m agl. To account for the decay of radon en route to the site, the land contact time calculations were weighted exponentially according to distance (in time) from LH.

$$\tau = \Delta t \sum_{i=1}^{N} \mathrm{e}^{-\lambda(t_N - t_i)}, \tag{2}$$

where Δt is the trajectory time-step and $i = 1, N$ represents all the trajectory points that are deemed to be 'in contact' with land. The distance-weighted time τ can be interpreted as the time required for a non-decaying scalar with the same surface flux density to achieve the same total column integral (R).

For air masses arriving at LH in summer, τ is typically less than 1 d (Fig. 5c). In contrast, τ values for air masses observed in July–September were frequently greater than 2 d. Large τ values are also evident in April and May, confirming that the lower wind speeds typical of this time of year lead to larger τ values than would otherwise be expected from the typical land fetch distance.

The bimodal form of the seasonal distribution of R (Fig. 5a) can thus largely be accounted for by variations in τ (Fig. 5c). This indicates that, at LH, seasonal changes in the time spent by an air mass in contact with the land surface have a larger influence on the observed seasonality in surface radon concentrations than do seasonal or regional changes in the terrestrial radon source function (Griffiths et al., 2010).

3.2.4. Variability of the 'effective' radon flux over the measurement fetch. Geographical and temporal variability in soil characteristics, soil moisture, wind speed and atmospheric pressure, can all result in changes to the terrestrial radon source function contributing to measured concentrations at LH on seasonal, or shorter, time-scales (Clements and Wilkening, 1974; Schery et al., 1984; Griffiths et al., 2010).

Prior to making landfall in south eastern Australia, most air masses en route to LH have either had a long fetch over the Southern Ocean or have spent a long time above the boundary layer. In either case, their corresponding initial radon concentrations are expected to be low (0.01–0.1 Bq m^{-3}, Gras and Whittlestone, 1992). Assuming that $R(t_o) \approx 0$ Bq m^{-3}, a distance-weighted mean 'effective' (or equivalent) radon flux density for the measurement fetch area can be estimated from

$$F_{\mathrm{eff}} = R/\tau. \tag{3}$$

F_{eff} represents the net sum of all contributions from radon sources and sinks (other than decay) along the trajectory followed by an idealized column of air. As some radon may be lost from the column due to ABL venting (entrainment) and other effects, it is important to note that our F_{eff} estimates may underrepresent radon surface flux densities for their respective fetch regions.

Mean monthly F_{eff} values are presented in Fig. 5d. Also shown is an estimate of the surface radon flux density at the LH site, calculated as an average of nine separate measurements collected at different locations around the site between April and June 2008 using an accumulation chamber (Zahorowski and Whittlestone, 1996).

Considerable variability (more than a factor of 2) is evident in F_{eff} between the warmer and cooler months of the year. For November–February, F_{eff} values are low, but in close agreement with the local flux density estimates. The land fetch during these periods is pre-dominantly near coastal (Fig. 4). F_{eff} values are highest for April–June, and September, when terrestrial fetch is mainly inland and varies from NW to SSW. Lower F_{eff} values in July and August corresponded to a period of the year when a uniformly western fetch pre-dominates (winter, Fig. 4a). The regional variability in radon flux density indicated here is broadly consistent with recently published findings of Griffiths et al. (2010), who noted low radon flux densities in coastal areas and across an extended inland region directly west of the Sydney basin. The authors would like to reiterate, however, that the calculation in (3) does not account for any seasonal changes in mean monthly ABL ventilation rates, which may also be significant.

3.3. Seasonal variability in nocturnal gradients

Radon gradients (ΔC) between 2 and 50 m exhibit a high variability on timescales from hours to seasons. Afternoon gradients are generally small, due to strong convective mixing through the deep daytime ABL, and most of the variability occurs in the nocturnal sampling window. For our monthly analysis of radon gradients, we chose to focus on the pre-dawn maximum gradient, ΔC_{max}. A detailed examination of the entire diurnal ΔC pattern is provided in the next section.

The seasonal cycle of ΔC_{max} at LH (Fig. 6a) looks very different to that of the afternoon minimum concentrations (Fig. 2). This is because the act of vertical differencing tends to eliminate or reduce the signal associated with horizontal advection, making ΔC_{max} largely insensitive to the fetch effects discussed in the previous section. Instead, ΔC_{max} reflects the degree of local accumulation of radon in the layer below 50 m, which is a function of the strength and extent of vertical mixing, and the surface flux density.

3.3.1. Vertical mixing. Vertical mixing is pre-dominantly a function of the local meteorological conditions near the surface, in particular wind stress and thermal stability.

ΔC_{max} at LH is characterized by low values in winter months, high values in both autumn and spring and intermediate values in summer (Fig. 6a). Roughly speaking, this pattern varies inversely to the monthly mean nocturnal wind speed (Fig. 6b; closed circles), highlighting the sensitivity of ΔC to

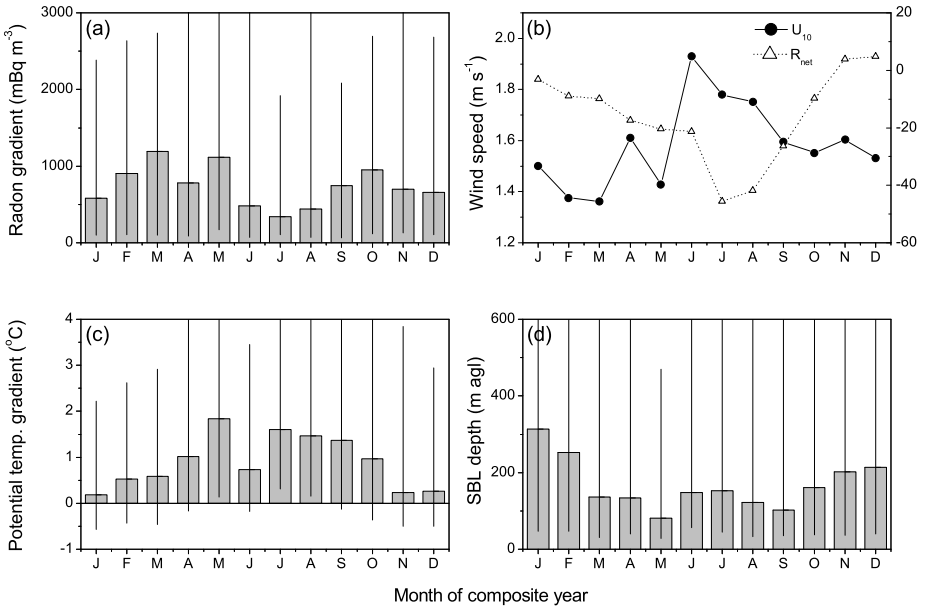

Fig. 6. (a) Monthly distributions (10th/50th/90th percentiles) of nocturnal $\Delta C_{\max}$, (b) monthly mean wind speed and net radiation in the nocturnal window, (c) monthly distributions of maximum $\Delta\theta$ in the pre-dawn window and (d) monthly distributions of LAPS nocturnal stable boundary layer depth in the pre-dawn window.

mechanical mixing. However, thermal stability effects further refine this relationship.

Figure 6c shows monthly distributions (10th/50th/90th percentiles) of the maximum potential temperature gradient between 2 and 50 m ($\Delta\theta_{\max}$) in the pre-dawn sampling window. The seasonal cycle of $\Delta\theta_{\max}$ is characterized by low values in November–January and generally higher values in April–September, with the exception of a negative anomaly in June. From November to January, night skies are frequently overcast due to the prevalence of onshore flows and moist air masses. This results in near-zero median nocturnal net radiation values (open triangles in Fig. 6b), which reduces the rate of surface cooling in these months. Between April and September, night skies are more frequently clear at LH, resulting in relatively large radiative heat loss (Fig. 6b) and larger near-surface temperature gradients (see also Moses et al., 1960; Servant, 1966; Dueñas et al., 1996; Kataoka et al., 2003). The June temperature gradient anomaly corresponds to a high mean nocturnal wind speed for that month, together with a moderate net radiation.

The observed $\Delta C_{\max}$ seasonal cycle thus results from an interplay between wind stress and thermal effects at night, with high $\Delta C_{\max}$ values occurring when both $\Delta\theta_{\max}$ is high and U_{10} is low (autumn and spring), and low values occurring either when U_{10} is high (winter) or when $\Delta\theta_{\max}$ is low (summer).

As radon is distributed through the SBL, ΔC can be considered to be an inverse proxy for SBL depth (Leach and Chandler, 1992; Allegrini et al., 1994; Guedalia et al., 1980; Hsu et al., 1980). Indeed, median monthly $\Delta C_{\max}$ values are found to vary inversely with the corresponding median SBL depths in the pre-dawn window, extracted from the LAPS model (Fig. 6d). Consistently low LAPS SBL depths occur in May, when wind speeds are moderate and night skies frequently clear (large $\Delta\theta_{\max}$); these are found to have high $\Delta C_{\max}$ values. Conversely, consistently deep SBLs tend to occur in January, and are associated with moderate wind speeds and weak temperature gradients; these tend to have small $\Delta C_{\max}$ values.

3.3.2. Local flux footprint. $\Delta C_{\max}$ is proportional to the surface radon flux density within the nocturnal turbulence footprint. As discussed in the introduction, this flux density can usually be assumed to be constant in time. However, as the local flux footprint varies with wind direction, wind speed and stability, small horizontal variations in the local surface radon flux density may influence the values of $\Delta C_{\max}$.

On stable nights with low wind speeds, the observed ΔC is primarily generated via radon accumulating near the surface from sources within a close distance of the site (say, 10–40 km, based on typical wind speeds of stable nights). There is evidence in the literature indicating that concentration measurement footprints exceed flux footprints under stable nocturnal conditions, and can be in the order of tens of kilometres (e.g. Vesala et al., 2008, and references therein). Since nocturnal wind directions in summer are typically S to SSE (Fig. 3b) and the LH land fetch is only 20–30 km in those directions, it is possible that the 'local' radon flux footprint sometimes includes a small oceanic component. This would lead to a reduced effective nocturnal radon surface source, which may contribute to the lower observed ΔC values at that time of year. Maximum nocturnal ΔC values measured on stable nights with an easterly component of wind direction

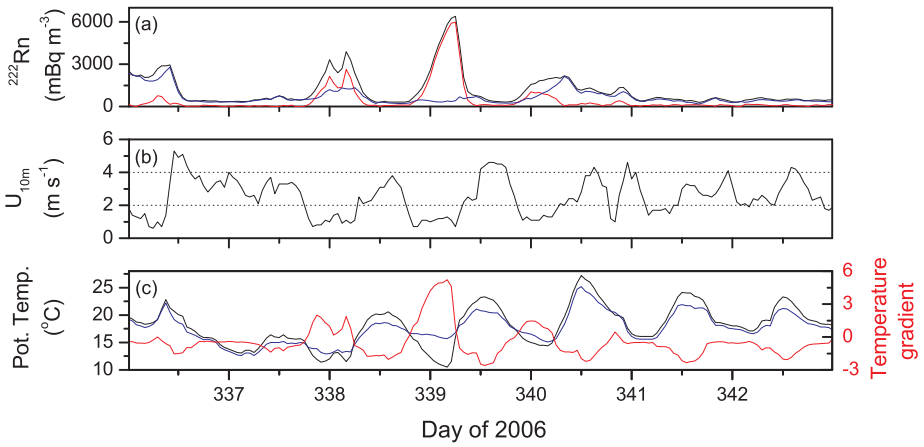

Fig. 7. 1 week of hourly observations at LH in 2006 spanning a range of meteorological conditions. (a) Radon concentration at 2 m (black), 50 m (blue) and ΔC (red), (b) 10 m wind speed and (c) potential temperature at 2 m (black), 50 m (blue) and $\Delta\theta$ (red).

(onshore flow) were, on average, 23% smaller than corresponding gradients observed under terrestrial fetch conditions. Part of this difference may thus be attributed to a reduced effective local flux density footprint caused by a combination of (a) a partial oceanic component to the footprint and (b) a smaller terrestrial radon source function for coastal fetch east of the site (see Fig. 5d).

3.4. Diurnal cycle

Marked diurnal signals were observed in the hourly LH radon data. A 1-week sample of the multiyear data set is presented in Fig. 7. Clearly evident in this figure are the low radon and radon gradient values typical of afternoon conditions when near-surface mixing is strong and the ABL is deep. At night, 2 m radon and ΔC values are closely linked to wind speed and near-surface temperature gradients. The highest ΔC values are observed on nights when strong temperature gradients coincide with low wind speeds (e.g. days 338, 339 and 340). On the most extreme case, day 339, the air aloft (50 m) became completely decoupled from the surface. Conversely, days 337, 341 and 342 demonstrate the low ΔC values associated with high wind speeds and low thermal stratification.

It is clear from the results presented here and in Section 3.3.1 that the pre-dominant and most direct factors influencing the radon gradient signal are the diurnal patterns of wind stress and thermal stability. These vary significantly in response to changes in local meteorological conditions modulated on meso to synoptic scales and greater (days to seasons).

In order to investigate diurnal patterns of vertical mixing more closely, we identified the set of all complete diurnal cycles in the data, and sorted them according to the strength of the radon gradient in the pre-dawn window. The resultant distribution of ΔC (not shown), is characterized by a very rapid rise to a broad maximum between 300 mBq m^{-3} (∼10th percentile) and 1000 mBq m^{-3} (∼50th percentile), followed by a slow quasi-logarithmic decay towards the high gradient values. Based on this form for the distribution, three categories of diurnal cycle were defined as follows:

(1) **Poorly mixed (high)**: radon gradient in the pre-dawn window was greater than or equal to the 50th percentile value (approx. 1000 mBq m^{-3});

(2) **Well mixed (low)**: radon gradient in the pre-dawn window was less than or equal to the 10th percentile value (approx. 300 mBq m^{-3}); and

(3) **Intermediate (medium)**: radon gradients between 10th and 50th percentiles.

Over flat terrain, Butterweck et al. (1994) adopted a similar classification scheme using radon concentrations at one altitude only (1.2 m). Their reasoning was that the radon concentration at a given height above a relatively constant source is directly related to the integrated diffusivity of the layers between the source and measurement height. As explained in the introduction, however, ΔC is a much more direct measure of vertical mixing and removes most of the background signal associated with horizontal advection and fetch-related source variations.

3.4.1. Asymptotic composites. Composite diurnal cycles for the two extreme radon gradient categories are contrasted in Fig. 8.

In the 'poorly mixed' category, the 2 m radon diurnal cycle is characterized by a pronounced morning maximum, typically within an hour of local sunrise, and an afternoon minimum (Fig. 8a). Similar cycles have been reported by Moses et al. (1960), Israël et al. (1966), Li (1974) and Butterweck et al. (1994). The 50 m radon diurnal cycle is relatively constant throughout the night, remaining close to the previous afternoon's minimum radon concentration until approximately 0500 h. The morning breakdown of the nocturnal inversion is evident from the rapid convergence of the 2 and 50 m radon signals

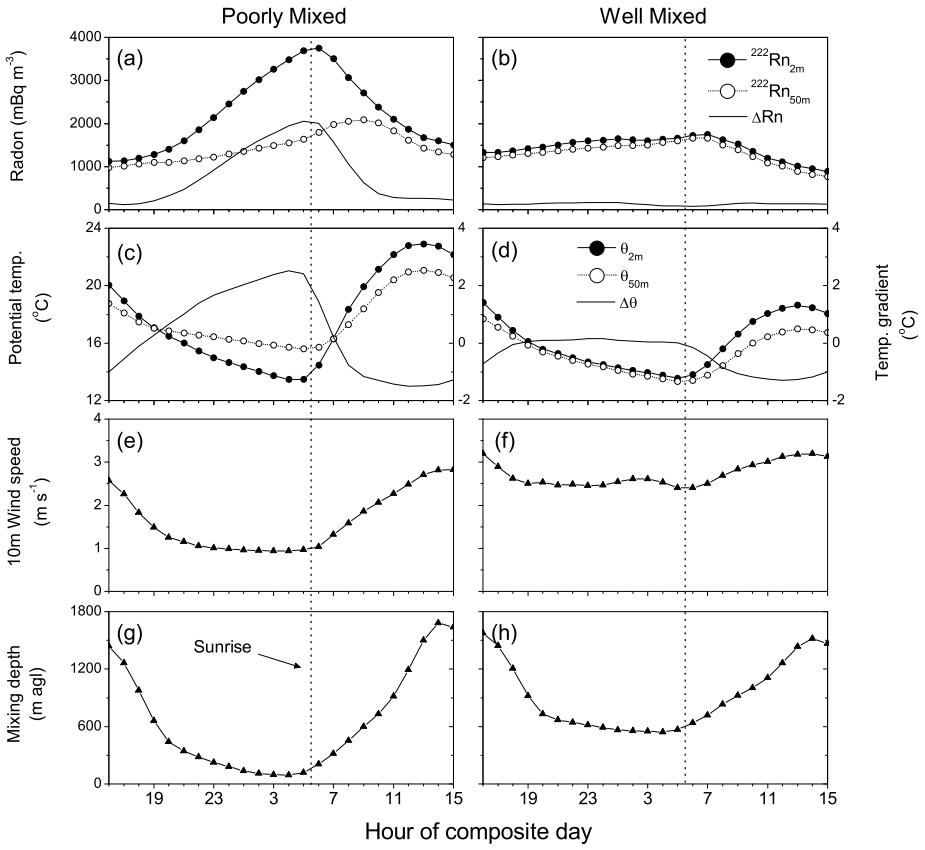

Fig. 8. Mean diurnal composites for days corresponding to poorly mixed and well-mixed conditions. (a,b) 2 and 50 m radon concentrations and gradient, (c,d) 2 and 50 m potential temperatures and gradient, (e,f) 10 m wind speed and (g,h) LAPS mixing depth. Filled circles, hollow circles and lines represent 2 m, 50 m and gradient observations, respectively. See text for details.

after sunrise, with 50 m concentrations rising as radon is mixed upwards from below. From mid-morning, the 50 m radon concentration then gradually reduces again towards the afternoon minimum value as the mixing depth increases (Fig. 8g). Observations of delayed morning radon maxima with height have also been reported by Moses et al. (1960), Pearson and Moses (1966), Servant (1966) and Li (1974). ΔC increases monotonically from sunset to sunrise, indicating a progressive accumulation of radon near the surface at night with little being transported aloft. Immediately after sunrise, ΔC decreases rapidly towards the afternoon minimum value, resulting in a highly asymmetric nocturnal peak. The nights were characterized by a shallow LAPS mixing depth, low wind speeds ($U_{10} < 1$ m s^{-1}) and strong thermal stratification with temperature gradients increasing as the night progressed ($\Delta\theta_{\max} \approx 2.5^{\circ}$C) (Fig. 8c, for example). These results therefore confirm the expectation that the 'poorly mixed' category corresponds to diurnal cycles in which the nocturnal component constitutes a shallow, very stable boundary layer. The frequent decoupling of the 2 and 50 m observations indicates that the upper measurement was often made in non-turbulent air within the residual layer above the nocturnal inversion.

By contrast, in 'well mixed' conditions, the 2 and 50 m radon diurnal cycles are almost identical (Fig. 8b); both are characterized by a slight increase in concentration, peaking approximately 1 h after sunrise, and a gradual decrease into the afternoon. The 2–50 m radon gradients were consequently small, averaging approximately 90 mBq m^{-3}. On these nights, the potential temperature gradient was negligible (Fig. 8d) and the hourly mean 10 m wind speed was rarely less than 2.5 m s^{-1} (Fig. 8f). LAPS nocturnal mixing depths remained high, with the average minimum only dropping to 580 m agl (Figs 8h). The 'well mixed' category therefore corresponds to deep neutral nocturnal boundary layers.

On 'intermediate' gradient nights (not shown), radon concentrations at both 2 and 50 m rose as the night progressed. This is consistent with both measurement heights being within the SBL. On average, ΔC values on these nights increased gradually after sunset, but then plateaued for 4–5 h in the late night, indicating that steady-state mixing conditions were achieved below 50 m. Gogolak and Beck (1980) also reported steady-state mixing conditions being achieved below 25 m by 3–4 h after sunset during their brief observation period. Rates of mixing increased again after sunrise.

Table 2. Distributions (10th, 50th, 90th percentiles) of radon gradients and meteorological quantities based on hourly measurements within the pre-dawn sampling window for the three gradient categories defined in the text

	High gradient			Intermediate gradient			Low gradient			
Qty.	10th	50th	90th	10th	50th	90th	10th	50th	90th	units
ΔC	905	1584	3226	152	462	873	0	91	204	mBq m^{-3}
U_{10}	0.48	0.92	1.48	0.63	1.23	2.43	1.31	2.24	3.8	m s^{-1}
$\Delta\theta$	−0.48	1.58	5.12	−0.62	0.33	1.94	−0.72	−0.30	0.59	°C
Zi_{LAPS}	28	70	294	39	176	710	98	572	1226	m agl
K_{B}	0.122	0.249	0.435	0.451	0.852	2.55	1.89	3.87	12.09	m^2 s^{-1}
Ri_{B}	−0.162	0.342	3.914	−0.175	0.039	0.317	−0.170	−0.020	0.055	
TKE	0.044	0.151	0.459	0.146	0.369	1.354	0.428	1.088	3.232	m^2 s^{-2}
σ_w	0.049	0.118	0.273	0.123	0.243	0.481	0.292	0.507	0.908	m s^{-1}
$\sigma_{u,v}/\sigma_w$	2.782	4.323	8.108	2.540	3.285	5.437	2.390	2.635	3.348	

Distributions (10th, 50th and 90th percentile values) of ΔC and other relevant quantities within the pre-dawn sampling window for all three diurnal cycle categories are summarized in Table 2.

3.4.2. Seasonal variability. A further decomposition of the stable (poorly mixed) category of diurnal cycles into summer and winter cases reveals some interesting differences (Fig. 9).

Overall, there is a shift in the mean radon concentrations to larger values in winter than summer (Figs 9a and b); this is mainly due to seasonal changes in fetch and contact time with land as discussed in Section 3.2. Also, nights on which the 2–50 m radon concentration gradient exceeded 1000 mBq m^{-3} in the pre-dawn window, characterized by consistently low wind speeds and clear skies, are more than three times as common in summer, largely attributable to seasonal changes in wind speed.

The 2 m radon signal exhibits a peak in concentrations within an hour of sunrise in both seasons (Figs 9a and b). However, in winter there is a longer period when radon concentrations are high. This is attributable to a combination of longer nights (up to 4 h less daylight: see net radiation composites in Figs 9g and h) and a delayed build-up of radon concentrations on summer evenings. The latter is primarily due to the effects of the summertime sea-breeze circulation. The wind direction composite on summer afternoons (Fig. 9e) remains consistently easterly until 2100–2300 h, after which it turns towards a more southerly direction. Wind speeds drop slowly until around 2200 h. Furthermore, the nocturnal mixing depth in summer (Fig. 9g) does not fall below 200 m until midnight, 5 h after the change in sign of net radiation, compared with 2000h in winter.

The 50 m radon diurnal cycle in summer exhibits a small gradual build-up from sunset to approximately 0500 h and slight post-sunrise maximum. In winter, however, the 50 m concentration remains relatively constant at near the afternoon minimum value until around 0500 h, followed by a pronounced post-sunrise maximum. These observations indicate that under poorly mixed conditions in summer the 50 m observations are near the top of, but still within, the stable nocturnal layer, whereas in winter the 50 m observations are clearly above the nocturnal inversion. Since nocturnal wind speeds were comparably low under poorly mixed conditions in each season (Figs 9e and f), this contrast in nocturnal mixing depth is most likely attributable to seasonal differences in thermal stability. This conclusion that is supported by the temperature composites, which show much larger temperature gradients in winter than in summer (Figs 9c and d).

3.4.3. Site influences. A conspicuous feature of the diurnal radon signal at LH is its low amplitude (peak to trough), the annual mean value of which was 1.49 Bq m^{-3} at 2 m. Despite LH being 18 km inland, the amplitude of its 2 m diurnal radon signal was comparable to measurements at our coastal site (Warrawong: 34°29′S, 150°52′E; 1.45 Bq m^{-3}). By comparison, the mean diurnal amplitudes of 2 m radon concentration at Richmond (33°36′S, 150°44′E; 55 km from the coast) and Muswellbrook (32°16′S, 150°53′E; 110 km from the coast) were 9.95 Bq m^{-3} and 12.19 Bq m^{-3}, respectively.

As discussed in Section 3.3.2, a pronounced marine influence on the LH radon signal may act to suppress nocturnal radon maxima (and hence the diurnal amplitude) when fetch is from the south or east. Furthermore, the topographic setting of LH is complex. With drops in elevation of up to 150 m within a 1 km radius of the site, drainage flows into the adjacent valleys could also be expected to suppress nocturnal radon maxima (Servant, 1966; Leach and Chandler, 1992; Kataoka et al., 2003).

A disparity between diurnal amplitudes of near-surface radon observations over flat versus complex or coastal sites is also evident in the literature. Butterweck et al. (1994) and Nagaraja et al. (2003) reported diurnal amplitudes of >50 Bq m^{-3} at 1 m over relatively flat ground, and an amplitude of 33 Bq m^{-3} was reported by Moses et al. (1960). By contrast, Li (1974) reported a diurnal amplitude of only 3.2 Bq m^{-3} at 6 m over complex terrain, and Dueñas et al. (1996) reported a diurnal amplitude of

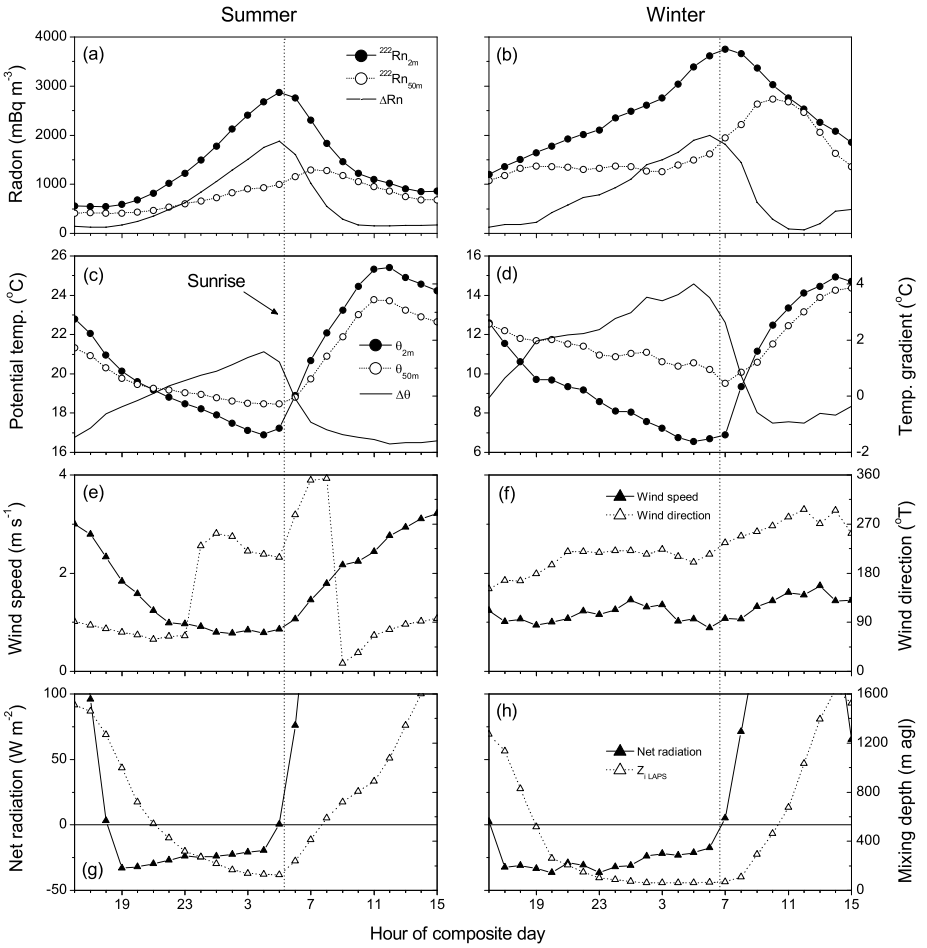

Fig. 9. Seasonal variability of diurnal composites in poorly mixed nocturnal conditions: (a,b) 2 and 50 m radon concentrations and gradient, (c,d) 2 and 50 m potential temperatures and gradient, (e,f) 10 m wind speed and direction and (g,h) net radiation and LAPS mixing depth.

1.2 Bq m^{-3} at a near coastal site. With the exception of Nagaraja et al. (2003) however, these statistics represent only days to months of observations, not an average of the complete annual cycle.

3.5. Nocturnal mixing patterns

The large variability seen in the radon and radon gradient observations discussed in Sections 3.3 and 3.4 is generated primarily by changes in the strength and depth of nighttime turbulent mixing. Focusing exclusively on the nocturnal window, we now briefly investigate the relationship between radon-derived measures of vertical mixing in the SBL, the drivers of that mixing and statistics of the turbulence itself.

For the following analysis we utilize the same categorization of diurnal cycles introduced in Section 3.4, including results from the third 'intermediate' category that has not yet been used. Nights in our data set that included the passage of a frontal system or apparent sharp change in fetch (as evidenced by a step change in the radon time series) were excluded; as were nights with discontinuous data. From the 942 possible nights, 698 were retained for the current analysis.

3.5.1. Bulk diffusivities in the pre-dawn window. If the surface radon flux density, F_s, within the local turbulence footprint is well known from independent measurements, then a bulk diffusivity parameter (K_B) can be calculated by inversion of a bulk diffusion relationship.

$$F_s = -K_B \frac{\Delta C}{\Delta z}. \tag{4}$$

K_B is a robust and useful measure of the integrated strength of mixing across the layer of interest (Servant, 1966; Hosler, 1969; Cohen et al., 1972; Trumbore et al., 1990).

The mean radon flux density in the vicinity of LH is 8.2 mBq m^{-2} s^{-1} (see Fig. 5d). Substituting this into eq. 4, K_B estimates were made in the pre-dawn sampling window, based on ΔC_{max} values in each of the three gradient categories (see Section 3.4). The low gradient ('well mixed') nights were associated with a

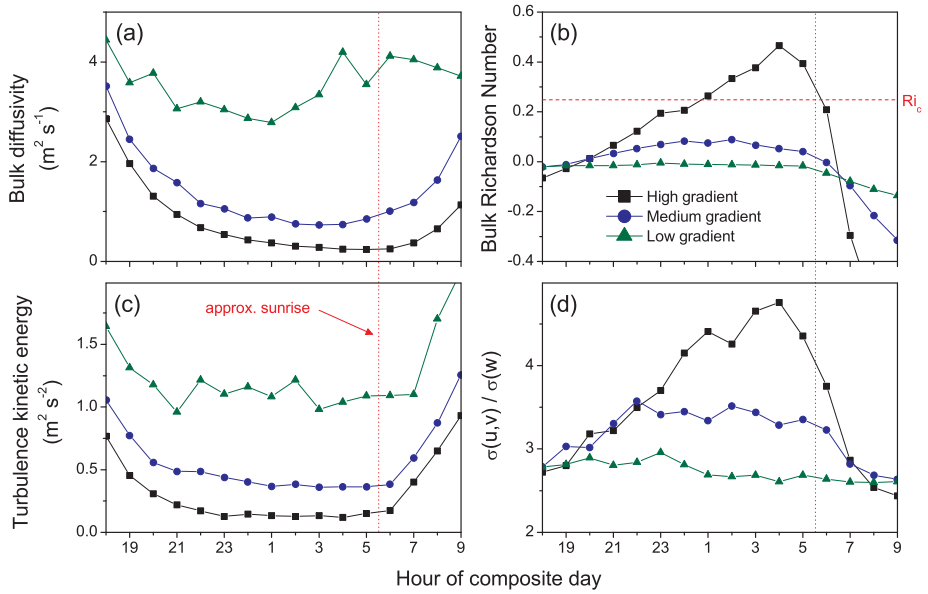

Fig. 10. Nocturnal composite plots of (a) 2–50 m radon-derived bulk diffusivity, (b) 2–50 m bulk Richardson number, (c) 50 m turbulence kinetic energy and (d) 50 m $\sigma_{(u,v)}/\sigma_{(w)}$, for high, medium and low radon gradient categories.

median bulk diffusivity of $K_B \sim 3.9$ m^2 s^{-1}, while high gradient ('poorly mixed') nights had $K_B \sim 0.25$ m^2 s^{-1}.

Hosler (1969) used a similar technique to derive K_B estimates for a 90 m layer adjacent to the surface, based on 22 months of intermittent radon observations at a semirural site in Washington D.C. For conditions ranging from near neutral to moderately stable, his estimates of K_B varied from 0.6 to 4.8 m^2 s^{-1}. These values are consistent with K_B estimates in this study under Intermediate and Low Gradient conditions (Table 2). Druilhet et al. (1980) reported seasonal changes in mean nocturnal diffusivities between 1.5 and 30 m agl based on 2 yr of 2 hourly radon observations in Roissy, France. K_B estimates at midnight ranged from 0.002 m^2 s^{-1} in summer, when conditions were most stable, to 0.15 m^2 s^{-1} in winter. These estimates are considerably lower than found in this study, but they were derived over flatter terrain and for a thinner atmospheric layer. K_B is known to vary with layer thickness and surface roughness (Moses et al., 1960; Jacobi and Andre, 1963; Hosler, 1969; Cohen et al., 1972; Druilhet et al., 1980). Servant (1966) estimated the K_B over a 100-m layer under various meteorological conditions over 7 d. K_B values obtained between 0000 and 0600h varied from 0.01 to 1 m^2 s^{-1}.

3.5.2. Turbulence and bulk mixing measures. The radon-derived K_B (eq. 4), represents an independent measure of the integrated result of vertical mixing processes within the layer of interest. This mixing is accomplished via the action of turbulence and modulated by wind stress and thermal stability. In this final results section, we will briefly explore the relationship between K_B, stability and turbulence.

In Fig. 10, the nocturnal composite median K_B in the three radon gradient categories is presented alongside the Ri_B:

$$Ri_B = \left(\frac{g}{\overline{\theta_v}}\right)\left(\frac{\Delta\theta_v}{\Delta U^2}\right)\Delta z, \tag{5}$$

where θ_v is the virtual potential temperature, g is gravity, U is the wind speed, z is height agl and Δ represents a gradient between 2 and 50 m. Ri_B is an appropriate stability parameter for comparison with K_B, as they are both bulk quantities computed over the same layer. In very stable conditions, Ri is a more suitable choice of stability parameter than that based on the Obukhov length (L), as L is a function of the turbulence itself and can be dominated by errors when turbulence levels are very low (Mahrt and Vickers, 2006; Banta et al., 2007). Hosler (1969), Cohen et al. (1972) and Leach and Chandler (1992) also advocate the Richardson number as an appropriate stability benchmark for evaluating near-surface radon gradients.

The interplay between bulk stability and integrated vertical mixing is very clear in Fig. 10. On nights when the highest radon gradients are observed, K_B drops to very low values in the first few hours after sunset, and then remains low for the remainder of the night. At the same time, Ri_B rises over the course of the night to reach values that are substantially greater than the 'critical' value (usually taken as $R_c \approx 0.25$), indicating strong suppression of vertical turbulence by thermal stratification. On medium gradient nights, however, K_B still drops to quite small values, despite the fact that Ri_B does not climb above ~0.1 (below R_c). This indicates that even moderately stable conditions are enough to substantially suppress vertical turbulence. Finally,

on low gradient nights Ri_B remains close to zero (indicating near-neutral stability) and K_B values are high all night. On both high and medium gradient nights, after sunrise Ri_B drops sharply to negative values (indicating unstable conditions) and K_B rises. Cohen et al. (1972) also found a strong relationship between the 6 and 270 m radon gradient and a stability parameter based on the Richardson Number.

Figures 10c and d present turbulence statistics from the three-dimensional sonic anemometer data at 50 m, computed in hourly bins and composited to match the results from the bulk quantities. This improves upon the work of Li (1974), who used the standard deviation of horizontal wind components as a TKE proxy to characterize the dependence of radon observations at 6 m on turbulence levels. Figure 10c shows turbulence kinetic energy (TKE) per unit mass:

$$\frac{\mathrm{TKE}}{m} = \frac{1}{2}\left(\overline{u'^2} + \overline{v'^2} + \overline{w'^2}\right) = \frac{1}{2}\left(\sigma_{u,v}^2 + \sigma_w^2\right), \quad (6)$$

where m is mass, and $[u', v', w']$ are components of the 3-D turbulent velocity vector. Comparing this plot with Fig. 10a, it is clear that there is a very close correspondence between the nocturnal evolution of the radon-derived K_B and the TKE at 50 m. Both K_B and TKE exhibit consistently low values on nights when the highest ΔC values were observed, and high values on low ΔC nights. On 'intermediate' (medium gradient) nights, both K_B and TKE drop to relatively low values (in contrast to the situation described in the Ri_B comparison).

Thermal stratification acts to suppress the vertical component of turbulence much more strongly than the horizontal components. To indicate the relative contributions of vertical and horizontal motions to the total TKE, Fig. 10d shows the ratio between the median hourly standard deviations of the horizontal and vertical velocity components at 50 m ($\sigma_{u,v}/\sigma_w$). In strong mixing conditions (low ΔC), this ratio is around 2.6−2.8, and changes little throughout the night. In medium and high ΔC conditions, however, the velocity ratio increases as the night progresses; in the high ΔC category, it reaches values of almost 5 in the pre-dawn hours. This 'flattening' of turbulence motions into pre-dominantly horizontal flows as thermal stratification increases (cf. Fig. 10b) is a well-known feature of very stable boundary layers, and is expected to be strongest at sites in complex terrain, where down-slope gravity currents and other mesoscale motions can form, resulting in significant horizontal contributions to the TKE (e.g. see review by Mahrt, 1999).

The results in this section confirm that the radon-derived K_B is an unambiguous measure of integrated vertical mixing in the SBL, and qualitatively demonstrates its ability to reveal important mixing relationships that are not illuminated using traditional stability parameters. A more quantitative investigation of these relationships is beyond the scope of this paper and will be reported in a subsequent study.

4. Summary and conclusions

Atmospheric radon-222 has long been employed as a tracer in both long-distance air mass transport and vertical mixing studies. For practical reasons, direct radon measurements with a high vertical and temporal resolution are only viable over short time periods (days to weeks). This restricts our ability to use radon to robustly characterize vertical mixing over the full spectrum of meteorological conditions occurring at a given site on diurnal to seasonal timescales. In this study, we have demonstrated that hourly radon measurements at two heights (2 and 50 m) offer a productive compromise to high vertical resolution measurements in that part of the atmosphere accessible by towers, and can be sustained routinely over long periods of time (more than 2 yr). The data set presented is unique in terms of its temporal coverage, temporal resolution, continuity, detector sensitivity, range of weather conditions represented and supporting meteorological measurements.

With the help of model-derived backtrajectories and boundary layer depths, we were able to characterize the pronounced seasonal variability in afternoon surface radon concentrations in the Sydney region in terms of air mass fetch, contact time with land, ABL dilution and regional variability of the radon source function. Influences of coastal sea breeze circulations and the local topography were identified, superimposed upon the dominant seasonal variations in regional circulation patterns.

Focussing on the nocturnal pre-dawn window, we then examined the two-point radon gradient (ΔC) data. The seasonal variability of nighttime ΔC is very different to that of the surface radon concentrations, as it is mainly influenced by the strength of vertical mixing and, to a lesser extent, variations in the local flux density footprint. As mixing is mainly forced by vertical variations in the wind stress and thermal stability on subdiurnal timescales, and largely independent of horizontal advection, it was appropriate to divide the data set into discrete diurnal cycles and categorize them according to the maximum observed nocturnal radon gradient. When this was done, strong and consistent relationships were identified between the observed radon signals, wind and temperature gradients and conventional measures of mixing and turbulence including the Ri_B and the TKE.

The radon-derived K_B, was found to be a robust and useful measure of the integrated strength of mixing across the layer of interest. Comparison of Ri_B and TKE with K_B verifies that strong relationships exist between thermal stability, turbulence intensity and the resultant mixing. Ri_B is an (bulk) indicator of the potential/forcing for mixing within the layer, whereas K_B is a measure of the integrated result of that mixing. On nights with very large ΔC (low K_B), TKE levels were found to be extremely low and Ri_B was well above the 'critical' value of 0.25. Under these conditions, the ratio of horizontal to vertical wind perturbations (standard deviations) was high, indicating 'flattening' of the turbulence into pre-dominantly horizontal flows. On the other hand, when ΔC was very small (high K_B), TKE levels were

high and Ri_B was near zero. In the middle ΔC category, however, both TKE levels and K_B indicated significantly reduced mixing, while Ri_B values remained below 0.1. It therefore appears that the $K_B - Ri_B$ relationship is non-linear, with only mildly stable conditions being sufficient to significantly suppress mixing. A more quantitative investigation of the relationships between radon gradients and nocturnal mixing processes will be reported in a subsequent study.

Hourly two-point radon gradients provide a direct, unambiguous measure of vertical mixing in the lower atmosphere, with the majority of background signals associated with horizontal advection and fetch-related source variations automatically removed by the differencing process. In addition to the information regarding regional transport and boundary layer dilution that can be extracted from analyses of single-point measurements, two-point radon gradient data sets provide a powerful new tool for routine verification of near-surface mixing processes in a range of models.

Acknowledgments

The authors would like to thank Mr. Ot Sisoutham for his role in the construction and field deployment of the radon detectors used in this study, and Mr. Sylvester Werczynski for developing the Visual Basic data logging software and backtrajectory analysis tools. We are also grateful to both anonymous reviewers for their constructive feedback.

References

Allegrini, I., Febo, A., Pasini, A. and Schiarini, S. 1994. Monitoring of the nocturnal mixed layer by means of particulate radon progeny measurement. *J. Geophys. Res.* **99**, 18 765–18 777.

Banta, R. M., Mahrt, L., Vickers, D., Sun, J., Balsley, B. B. and co-authors. 2007. The very stable boundary layer on nights with weak low-level jets. *J. Atmos. Sci.* **64**, 3068–3090.

Beck, H. L. and Gogolak, C. V. 1979. Time-dependent calculations of the vertical distribution of ^{222}Rn and its decay products in the atmosphere. *J. Geophys. Res.* **84**, 3139–3148.

Butterweck, G., Reineking, A., Kesten, J. and Porstendorfer, J. 1994. The use of the natural radioactive noble gases radon and thoron as tracers for the study of turbulent exchange in the atmospheric boundary layer: case study in and above a wheat field. *Atmos. Environ.* **28**, 1963–1969.

Clements, W. E. and Wilkening, M. H. 1974. Atmospheric pressure effects on ^{222}Rn transport across the earth-air interface. *J. Geophys. Res.* **79**, 2654–2668.

Cohen, L. D., Barr, S., Krablin, R. and Newstein, H. 1972. Steady-state vertical turbulent diffusion of radon. *J. Geophys. Res.* **77**, 2654–2668.

Draxler, R. R. and Hess, G. D. 1998. An overview of the HYSPLIT-4 modelling system for trajectories, dispersion and deposition. *Aust. Meteorol. Mag.* **47**, 295–308.

Druilhet, A., Guedalia, D. and Fontan, J. 1980. Use of natural radioactive tracers for the determination of vertical exchanges in the planetary boundary layer. In: *Natural Radiation Environment III*. Volume 1 (eds. Thomas F. Gesell and Wayne M. Lowder). U. S. Department of Energy DOE Symposium series **51**, 226–241.

Dueñas, C., Pérez, M., Fernández, M. C. and Carretero, J. 1996. Radon concentrations in surface air and vertical atmospheric stability of the lower atmosphere. *J. Environ. Radioact.* **31**, 87–102.

Fernando, H. J. S. and Weil, J. C. 2010. Whither the stable boundary layer? A shift in the Research Agenda. *Bull. Am. Meteorol. Soc.* **91**, 1475–1484.

Fontan, J., Birot, A., Blanc, D., Bouville, A. and Druilhet, A. 1966. Measurement of the diffusion of radon, thoron and their radioactive daughter products in the lower layers of the Earth's atmosphere. *Tellus* **18**, 623–632.

Gogolak, C. V. and Beck, H. L. 1980. Diurnal variations of radon daughter concentrations in the lower atmosphere. In: *Natural Radiation Environment III*. Volume 1 (eds. Thomas F. Gesell and Wayne M. Lowder). U. S. Department of Energy DOE Symposium series **51**, 259–280.

Gras, L. L. and Whittlestone, S. 1992. Radon and CN: complementary tracers of polluted air masses at coastal and island sites. *J. Radioanal. Nucl. Chem.* **161**(1), 293–306.

Griffiths, A. D., Zahorowski, W., Element, A. and Werczynski, S. 2010. A map of radon flux at the Australian land surface. *Atmos. Chem. Phys.* **10**, 8969–8982, doi:10.5194/acp-10-8969-2010.

Guedalia, D., N'Tsila, A., Druilhet, A. and Fontan, J. 1980. Monitoring of the atmospheric stability above an urban and suburban site using sodar and radon measurements. *J. Appl. Meteorol.* **19**, 839–848.

Holtslag, A. A. M. and Boville, B. A. 1993. Local versus nonlocal boundary-layer diffusion in a global climate model. *J. Clim.* **6**, 1825–1842.

Hosler, C. R. 1968. Urban-rural climatology of atmospheric radon concentrations. *J. Geophys. Res.* **73**, 1155–1166.

Hosler, C. R. 1969. Vertical diffusivity from radon profiles. *J. Geophys. Res.* **74**, 7018–7026.

Hsu, S. A., Larson, R. E. and Bressan, D. J. 1980. Diurnal variations of radon and mixing heights along a coast: a case study (Gulf Coast). *J. Geophys. Res.* **85**, 4107–4110.

Israël, H. 1951. Radioactivity of the atmosphere. In: *Compendium of Meteorology* (ed. T. F. Malone). Am. Meteorol. Soc., Washington, DC, 155–161.

Israël, H., Hobert, M. and Israël, G. W. 1966. Results of continuous measurements of radon and its decay products in the lower atmosphere. *Tellus* **18**, 638–641.

Israelsson, S. 1978. Meteorological influences on atmospheric radioactivity and its effects on the electrical environment. In: *Natural Radiation Environment III*. Volume 1 (eds. Thomas F. Gesell and Wayne M. Lowder). U. S. Department of Energy DOE Symposium series; **51**, 210–225.

Jacobi, W. and Andre, K. 1963. The vertical distribution of Rn-222, Rn-220 and their decay products in the atmosphere. *J. Geophys. Res.* **68**, 3799–3814.

Kataoka, T., Yunoki, E., Shimizu, M., Mori, T., Tsukamoto, O. and co-authors. 2003. Concentrations of ^{222}Rn, its short-lived daughters and ^{212}Pb and their ratios under complex atmospheric conditions and topography. *Bound.-Layer Meteorol.* **107**, 219–249.

Kumar, A. V., Sitaraman, V., Oza, R. B. and Krishnamoorthy, T. M. 1999. Application of a numerical model for the planetary boundary

layer to the vertical distribution of radon and its daughter products. *Atmos. Environ.* **33**, 4717–4726.

Lambert, G., Polian, G., Sanak, J., Ardouin, B., Buisson, A. and co-authors. 1982. Cycle du radon et de ses descentants: application à l'étude des échanges troposphère-stratosphère. *Ann. Géophys.* **38**, 497–531.

Leach, V. A. and Chandler, W. P. 1992. Atmospheric dispersion of radon gas and its decay products under stable conditions in arid regions of Australia. *Environ. Monit. Assess.* **20**, 1–17.

Li, T.-Y. 1974. Diurnal variations of radon and meteorological variables near the ground. *Bound.-Layer Meteorol.* **7**, 185–198.

Mahrt, L. 1999. Stratified atmospheric boundary layers. *Bound.-Layer Meteorol.* **90**, 375–396.

Mahrt, L. and Vickers, D. 2006. Extremely weak mixing in stable conditions. *Bound.-Layer Meteorol.* **119**, 19–39.

Malakhov, S. G., Bakulin, V. N., Dmitrieva, G. V., Kirichenko, L. V., Sisigina, T. L. and co-authors. 1966. Diurnal variations of radon and thoron decay product concentrations in the surface layer of the atmosphere and their washout by precipitations. *Tellus* **18**, 643–654.

Martens, C. S., Shay, T. J., Mendlovitz, H. P., Matross, D. M., Saleska, S. R. and co-authors. 2004. Radon fluxes in tropical forest ecosystems of Brazilian Amazonia: night-time CO_2 net ecosystem exchange derived from radon and eddy covariance methods. *Glob. Change Biol.* **10**, 618–629.

Moses, H., Stehney, A. F. and Lucas, H. F. J. 1960. The effect of meteorological variables upon the vertical and temporal distributions of atmospheric radon. *J. Geophys. Res.* **65**, 1223–1238.

Nagaraja, K., Prasad, B. S. N., Madhava, M. S., Chandrashekara, M. S., Paramesh, L. and co-authors. 2003. Radon and its short-lived progeny: variations near the ground. *Radiat. Meas.* **36**, 413–417.

Newstein, H., Cohen, L. D. and Krablin, R. 1971. An automated atmospheric radon sampling system. *Atmos. Environ.* **5**, 175–181.

Pearson, J.E. and Moses, H. 1966. Atmospheric radon-222 concentration variation with height and time. *J. Appl. Meteorol.* **5**, 175–181.

Perrino, C., Catrambone, M. and Pietrodangelo, A. 2008. Influence of atmospheric stability on the mass concentration and chemical composition of atmospheric particles: a case study in Rome, Italy. *Environ. Int.* **34**, 621–628.

Porstendorfer, J., Butterweck, G. and Reineking, A. 1991. Diurnal variation of the concentrations of radon and its short-lived daughters in the atmosphere near the ground. *Atmos. Environ.* **25A**, 709–713.

Puri, K., Dietachmayer, G. S., Mills, G. A., Davidson, N. E., Bowen, R. A. and co-authors. 1998. The new BMRC Limited Area Prediction System, LAPS. *Aust. Meteorol. Mag.* **47**, 203–223.

Schery, S. D., Gaeddert, D. H. and Wilkening, M. H. 1984. Factors affecting exhalation of radon from a gravelly sandy loam. *J. Geophys. Res.* **89**, 7299–7309.

Servant, J. 1966. Temporal and spatial variations of the concentration of the short-lived decay products of radon in the lower atmosphere. *Tellus* **18**, 663–670.

Sisigina, T. L. 1964. Vertical distribution of radon in the boundary layer of the atmosphere (0–300m) in connection with changing meteorological conditions. *Izvest. Akad. Nauk. S. S. S. R. Ser. Geofiz.* **3**, 414–421.

Sorbjan, Z. 2006. Local structure of turbulence in stably stratified boundary layers. *J. Atmos. Sci.* **63**, 1526–1537.

Thomas, J. W. and Leclare, P. C. 1970. A study of the two-filter method for radon-222. *Health Phys.* **18**, 113–122.

Trumbore, S. E., Keller, M., Wofsy, S. C. and Da Costa, J. M. 1990. Measurements of soil and canopy exchange rates in the Amazon rain forest using ^{222}Rn. *J. Geophys. Res.* **95**, 16 865–16 873.

Turekian, K. K., Nozaki, Y. and Benninger, L. K. 1977. Geochemistry of atmospheric radon and radon products. *Ann. Rev. Earth Planet. Sci.* **5**, 227–255.

Ussler, W. I., Chanton, J. P., Kelley, C. A. and Martens, C. S. 1994. Radon 222 tracing of soil and forest canopy trace gas exchange in an open canopy boreal forest. *J. Geophys. Res.* **99**, 1953–1963.

Vesala, T., Kljun, N., Rannik, Ü., Rinne, J., Sogachev, A. and co-authors. 2008. Flux and concentration footprint modelling. *State of the Art Environmental Pollution* **152**, 653–666.

Wigand, A. and Wenk, F. 1928. Der gehalt der luft an radium-emanation, nach messungen bei flugzeugaufstiegen. *Ann. Lpz. Phys. (Annalen der Physik)* **86**, 657–686.

Wilkening, M. H. and Clements, W. E. 1975. Radon-222 from the ocean surface. *J. Geophys. Res.* **80**, 3829–3830.

Williams, A. G., Chambers, S. D., Zahorowski, W., Crawford, J., Matsumoto, K. and co-authors. 2009. Estimating the Asian radon flux density and its latitudinal gradient in winter using ground-based radon observations at Sado Island. *Tellus* **61B**, 732–746.

Williams, A. G., Zahorowski, W., Chambers, S. D. and Griffiths, A. 2011. The vertical distribution of radon in clear and cloudy daytime terrestrial boundary layers. *J. Atmos. Sci.* **68**, 155–174.

Zahorowski, W. and Whittlestone, S. 1996. A fast portable emanometer for field measurement of radon and thoron flux. *Radiat. Prot. Dosim.* **67**, 109–120.

Zahorowski, W., Chambers, S., Wang, T., Kang, C.-H., Uno, I. and co-authors. 2005. Radon-222 in boundary layer and free tropospheric continental outflow events at three ACE-Asia sites. *Tellus* **57**, 124–140.